

Domain Structure and Boundary in Single-Layer Graphene Grown on Cu(111) and Cu(100) Films

Yui Ogawa,[†] Baoshan Hu,^{‡,§} Carlo M. Orofeo,[†] Masaharu Tsuji,^{†,‡} Ken-ichi Ikeda,[†] Seigi Mizuno,[†] Hiroki Hibino,^{||} and Hiroki Ago^{*,†,‡}

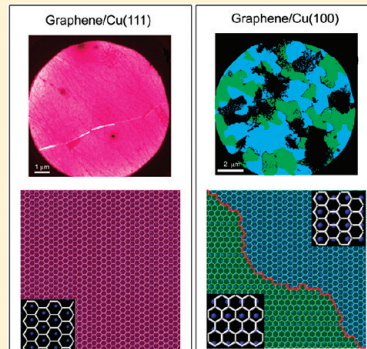
[†]Graduate School of Engineering Sciences and [‡]Institute for Materials Chemistry and Engineering, Kyushu University, Fukuoka 816-8580, Japan

[§]School of Chemistry and Chemical Engineering, Chongqing University, Chongqing 400044, P. R. China

^{||}NTT Basic Research Laboratories, NTT Corporation, Kanagawa 243-0198, Japan

Supporting Information

ABSTRACT: Size, orientation, and boundary of graphene domains are the current focus of chemical vapor deposition (CVD) growth because they are closely related to graphene's physical properties. Here, we study the domain structure of single-layer graphene grown by ambient pressure CVD over heteroepitaxial Cu(111) and Cu(100) films. Low energy electron microscope measurements reveal that the Cu(111) film gives uniform single-layer graphene whose orientation is consistent with the underlying Cu lattice for areas over 1 mm². On the other hand, single-layer graphene grown on Cu(100) film exhibits clear multidomain structure with two main orientations rotated by 30°. Moreover, a weak Raman D-band is observed along the domain boundaries for the graphene grown on the Cu(100). Our results give new insights into the growth mechanism of CVD-grown graphene over Cu metals and offer a new direction for the realization of single-crystalline graphene.



SECTION: Nanoparticles and Nanostructures

Graphene, a two-dimensional sheet of honeycomb carbon lattice, has attracted great interest because of its unique physical properties and potential applications in many fields.¹ In particular, electronic applications, such as transparent electrodes, high frequency transistors, and bendable devices, are expected due to extraordinary high carrier mobility, mechanical flexibility, and optical property.^{2–5} Among several methods to prepare graphene films including exfoliation of graphite,⁶ thermal evaporation of SiC crystals,^{4,7–9} chemical reduction of graphene oxide,^{10,11} and catalytic chemical vapor deposition (CVD) growth using transition metal films,^{2,12–17} CVD on Cu foils is one of the most promising and widely employed methods to produce large-area, single-layer graphene due to the low carbon solubility and low cost of Cu metal.^{2,17} However, recent works demonstrate that the single-layer graphene films are polycrystalline, consisting of a number of small graphene domains whose orientations are randomly distributed.^{18–23} Dark-field transmission electron microscope (TEM) analysis showed that the single-layer graphene formed on Cu foil is a patchwork of randomly oriented small domains with the size of 0.1–1 μm. This is closely related to the polycrystalline structure of the Cu foil. Moreover, the widely used Cu foil has a (100) square lattice, which is not suitable for epitaxial graphene growth due to mismatch of the lattice symmetry.

The graphene's domain structure and boundary are predicted to affect the carrier mobility,²⁴ chemical reactivity,²⁵ tension

strength,^{26,27} and magnetic property.²⁸ The polycrystalline CVD graphene shows a carrier mobility of a few hundred to a few thousand cm²/(V s) on SiO₂/Si,^{17,22} which is lower than that of mechanically exfoliated graphene (~10 000 cm²/(V s)).^{1,2} Thus, the direct observation of the domain structure is important, and moreover, tailoring the domain structure is an essential challenge for the control of physical properties of graphene. Recently, some groups synthesized large graphene domains through the optimization of the growth condition.^{29–31} The domain size reaches 10–500 μm on Cu foil, but the size is not still enough for the practical applications. Further, since the neighboring graphene domains formed at different Cu grains have different orientations of hexagons, it is challenging to connect the domains atomically at the boundaries.

On the other hand, orientation-controlled growth of graphene was achieved by an epitaxial CVD approach using heteroepitaxial Co,¹⁵ Ni,³² Cu,^{33,34} Ir,³⁵ and Ru^{36,37} which are deposited on single-crystal sapphire (α -Al₂O₃(0001)) or MgO(111) substrates. This approach gives crystalline metal films suitable for large-area graphene growth with much lower cost than pure single-crystalline metal films. The high crystallinity of the heteroepitaxial metal gives uniform single-

Received: November 25, 2011

Accepted: December 27, 2011

Published: December 27, 2011

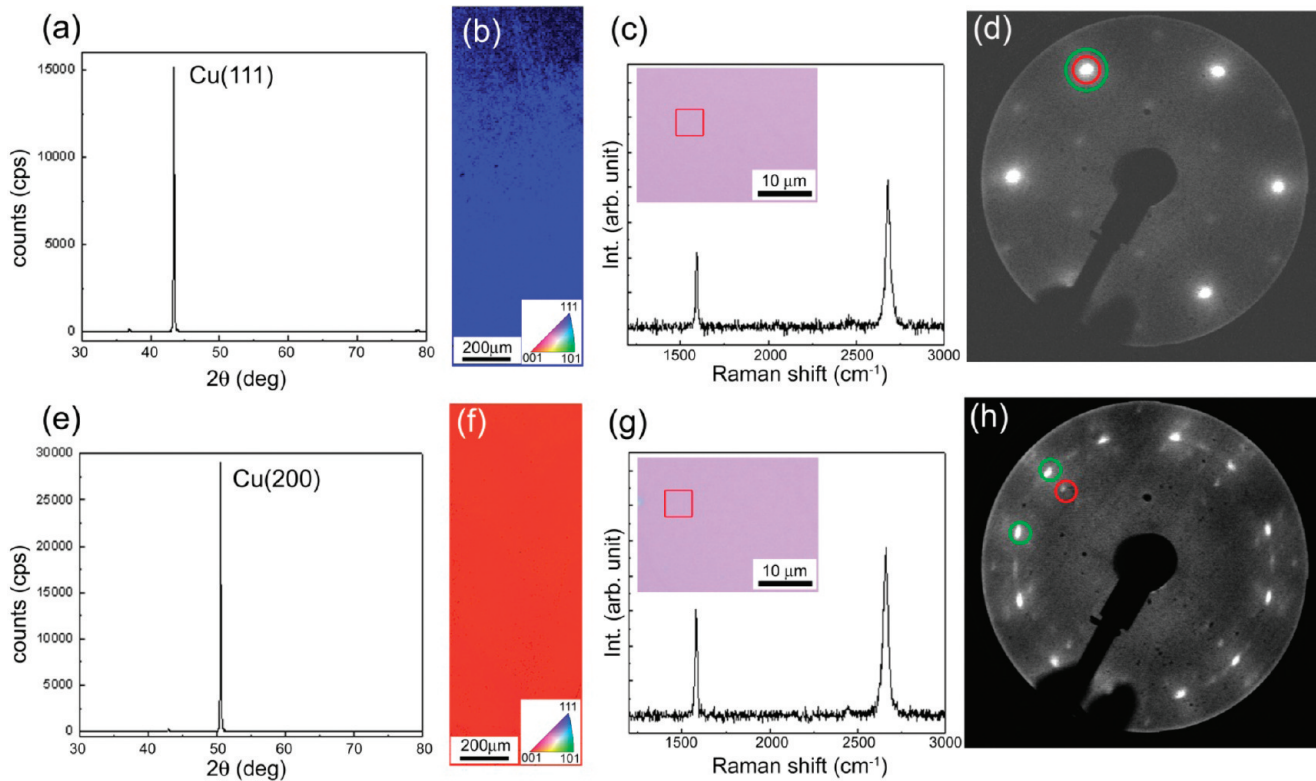


Figure 1. XRD profiles (a,e) and EBSD data (b,f) of Cu films measured after CVD. (c,g) Raman spectra and optical microscope images (inset) of graphene transferred on the SiO_2/Si substrate. (d,h) LEED images of as-grown graphene on Cu measured with 100 eV. The Cu films were deposited on $\text{MgO}(111)$ (a–d) and $\text{MgO}(100)$ (e–h) substrates. Red squares in (c,g) insets show the areas where Raman spectra were obtained. Green and red circles in (d,h) show the diffraction spots originating in graphene and the underlying Cu lattice, respectively.

layer graphene not only for low carbon solubility metals like Cu but also for Co and Ni whose carbon solubility is high.^{15,32} Our low energy electron diffraction (LEED) measurement with ~ 1 mm spot size proves that the average orientation of hexagons is controlled by this method,^{15,33} but microscopic domain structure has not been well understood. In addition, these previous studies only investigated the metal films with hexagonal closed packed structure (hcp) (0001) or face-centered cubic (fcc) (111) planes whose symmetry matched with the graphene structure but commonly used Cu foil has fcc (100) plane with 4-fold symmetry due to high temperature rolling process.^{21,22} Microscopic analysis, mainly scanning tunneling microscope (STM) observation, has been frequently used to determine the epitaxial relationship between CVD-grown graphene and underlying single-crystal Cu(111) or Cu(100) films. These works present periodic moiré structures which can be explained by the epitaxial relationship and lattice mismatch of graphene and the Cu metal.^{38–43} However, such a method is not applicable to wide area inspection, and a more systematic understanding is required. In addition, clarifying the influence of the Cu crystalline plane on graphene's domain structure is important for the understanding of the growth mechanism as well as to maximize graphene's physical properties for future electronic applications.

Here, we present domain structures of large-area, single-layer graphene films grown on heteroepitaxial Cu(111) and (100) films which are deposited on single-crystal MgO(111) and (100) substrates, respectively. The high-temperature sputtering onto the MgO substrates and further hydrogen annealing at the CVD temperature give single-crystalline Cu films. A low energy electron microscope (LEEM) is used to investigate the domain

structure for the as-grown graphene without a transfer process. By combination with Raman analysis, it is demonstrated that domain structure, domain size, and orientation are strongly influenced by the Cu crystalline plane and that the Cu(111) is preferable for the orientation-controlled graphene growth.

Heteroepitaxial Cu films were deposited on MgO(111) and (100) substrates at 500 °C by radio frequency (RF) magnetron sputtering. The graphene films were grown by ambient pressure CVD. After thermal annealing in H_2/Ar flow at 1000 °C to improve the metal crystallinity, the sample was reacted with a mixed gas of $\text{CH}_4/\text{H}_2/\text{Ar}$ flow at the same temperature to grow graphene on the Cu surface. The crystallinity of the Cu films was investigated by X-ray diffraction (XRD) and electron backscattered diffraction (EBSD) methods. A Cu film deposited on MgO(111) showed a sharp diffraction peak at $\sim 42^\circ$ assigned to Cu(111) diffraction (Figure 1a). The EBSD image clearly shows that the Cu film has a (111) plane normal to the substrate, and it is free from the metal grain boundary (Figure 1b). Especially, twin structures observed for the Cu film sputtered on sapphire at room temperature³⁵ are completely suppressed, resulting in high quality single-crystalline Cu(111) film due to high temperature sputtering and MgO crystal structure. The combined analyses of XRD and EBSD prove that the whole Cu film has Cu(111) single-crystal structure. Similarly, grain boundary-free single-crystalline Cu(100) film was successfully obtained on the MgO(100) substrate, as seen in Figure 1e,f.

The graphene film was transferred onto the target SiO_2/Si substrate using the polymethyl methacrylate (PMMA)-assisted etching method.¹⁵ Both graphene films transferred from Cu(111) and Cu(100) films showed characteristic Raman

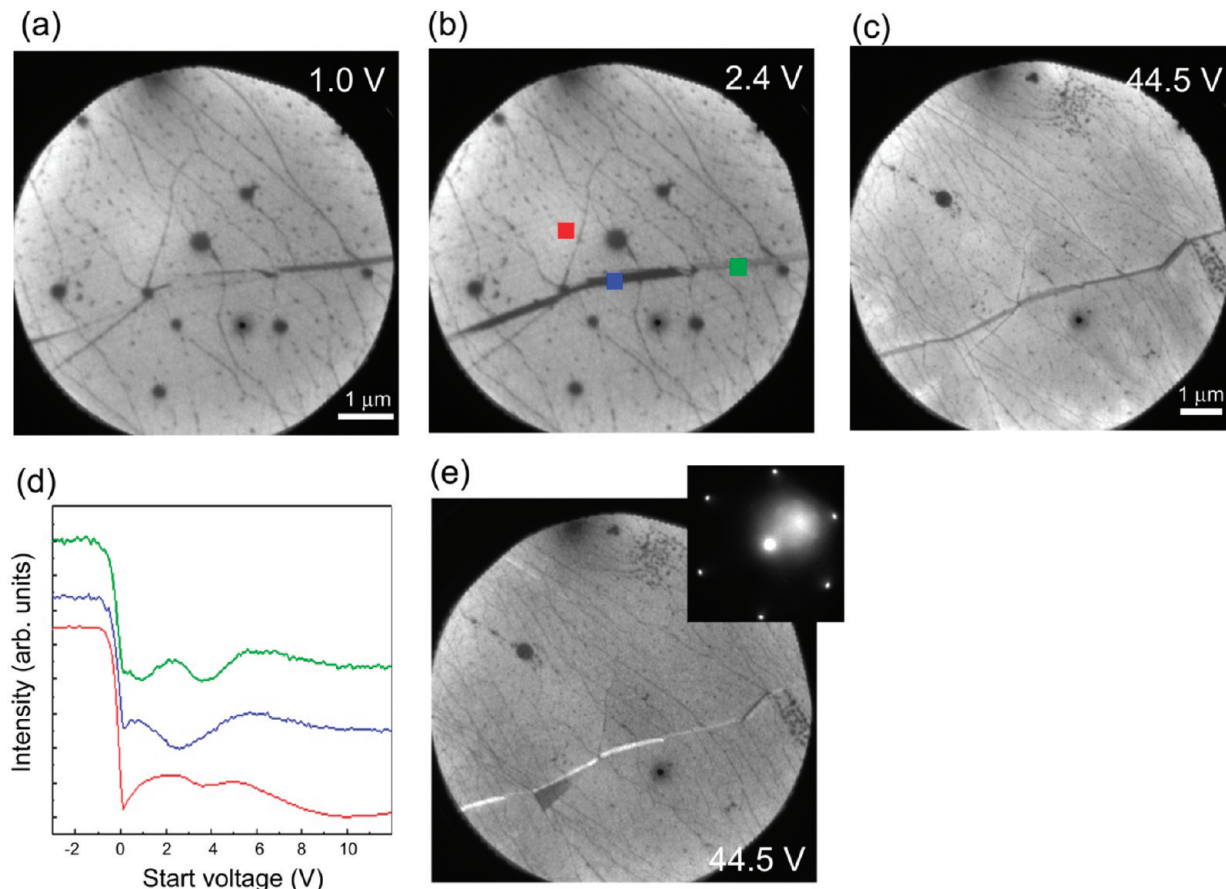


Figure 2. (a–c) BF LEEM images of as-grown graphene on heteroepitaxial Cu(111) measured with different electron energies. (d) Electron reflectivity data measured at points highlighted in (b). (e) DF LEEM image measured for the same area as (a–c) with the diffraction condition shown in the inset.

spectra of single-layer graphene (Figure 1c,g), stronger 2D-band intensity than the G-band ($I_{2D}/I_G \sim 1.5$), and a narrow 2D-band with $30\text{--}40\text{ cm}^{-1}$ width. The negligible defect-related D-band indicates that the graphene is of high quality.^{10,14} In addition, analysis of optical contrast also supports the single-layer graphene and uniformity of the film (insets of Figure 1c,g).^{44,45}

We investigated the orientation of the as-grown graphene on the Cu films by LEED. Shown in Figure 1d,h are LEED patterns measured with a 100 eV electron beam whose spot size is around 1 mm. The graphene formed on Cu/MgO(111) showed six sharp diffraction spots. The analysis of the energy dependence signified that these six peaks are originated in both the graphene lattice (green circle) and the Cu(111) lattice (red circle).¹⁵ This result proves that graphene is epitaxially formed on Cu(111)/MgO(111). Note that the Cu(111) lattice has 3-fold symmetry, while the graphene hexagonal lattice has 6-fold symmetry. Thus, at high electron energy (400 eV), three diffraction spots coming solely from the Cu(111) lattice became prominent (Supporting Information, SI-1a), again proving high crystallinity of the Cu film. For comparison, we also performed LEED measurement for the single-crystalline Cu(111) substrate after the surface cleaning process inside the LEED chamber (not shown here). The LEED pattern of the pure Cu(111) surface is almost identical to that of graphene/Cu(111). In addition, their $I-V$ curves of LEED patterns are essentially the same with those of graphene/Cu(111) except for the clear diffraction from graphene only at low incident

electron energies. These results indicate the absence of reconstruction of the Cu(111) surface due to graphene growth.

On the other hand, graphene/Cu(100)/MgO(100) showed a more complex LEED pattern (Figure 1h). There are two sets of diffraction patterns. We interpret that the outer 12 broad streaks (green circle) are originated from graphene and the inner four peaks (red) are from the Cu(100) lattice because the latter Cu(100) diffraction peaks are very sharp and become stronger with increasing the electron energy (Supporting Information, SI-1b). From the LEED pattern, we conclude that the graphene covers the Cu surface with two preferential [10] orientations with angles of $0 \pm 2^\circ$ and $30 \pm 2^\circ$ with respect to the underlying Cu[011] lattice. Wofford et al. reported the evolution of four-lobed graphene domains in association with the square Cu(100) lattice.²¹ Our result is consistent with their observations. Note that there also exists a weak and broad diffraction streak between the 0° and 30° positions corresponding to the mis-aligned graphene domains.

The above-mentioned crystalline-plane-dependent orientation of graphene hexagons is qualitatively consistent with the previous report.^{15,21} However, the LEED gives the averaged orientation of graphene domains existing in a large beam spot size (~ 1 mm), thus it lacks information on microscopic domain structure. Recently, spatial domain distribution was visualized by using dark-field TEM for single-layer graphene transferred from a Cu foil.^{18,19} Relatively small graphene domains up to several micrometers are observed for the large-area graphene sheet. TEM observation requires a transfer process by

dissolving the metal catalyst so that it is difficult to analyze the relative orientation of the graphene domain against the metal lattice. In addition, TEM is not suitable for large-area inspection, partly because the graphene surface can be contaminated with PMMA residue. Another tool is STM which gives an atomic resolution image of graphene on the metal. STM was used for atomic scale characterizations of single-layer graphene grown on Cu foil and single-crystalline Cu(111) and (100) films.^{38–43} However, the scan area is typically small, and it is not suitable for large-area statistic analysis.

To investigate the domain structure of the CVD-grown graphene, we measured LEEM for the graphene on the heteroepitaxial Cu films. Although the LEEM is used to analyze graphene formed on a metal catalyst and SiC substrate, the growth is usually done in an ultrahigh vacuum chamber.^{9,21} We measured the ex situ LEEM for the graphene grown by the ambient pressure CVD. This ambient pressure CVD is advantageous because it is applicable to large-scale graphene growth with low cost and suppresses thermal evaporation of Cu which is problematic in vacuum CVD. In addition, the LEEM does not require a graphene transfer process and can scan a large area by simply moving the sample stage. Moreover, the electron reflectivity enables determination of the graphene thickness.⁹

After introducing the as-grown sample into the LEEM chamber, the sample was annealed to remove the surface adsorbents in vacuum because of inevitable exposure to air during the transfer. We measured bright-field (BF) and dark-field (DF) images that are formed from the reflection and diffraction of electron beams, respectively. From BF LEEM measurement, the spatial distribution of the number of graphene layers is obtained from the electron reflectivity as a function of accelerating voltage. Shown in Figure 2a–c is BF LEEM images of as-grown graphene on heteroepitaxial Cu(111) measured at different electron energies. The BF image showed the uniform white contrast except for some dark spots and linear lines. The reflectivity data measured at three points of Figure 2b are displayed in Figure 2d. The white area (marked with a red square) shows a feature of single-layer graphene, indicating the formation of uniform single-layer graphene. The thick dark line observed at the center of Figure 2b (blue and green squares) is likely 2–3 layers of graphene. We interpret that this line represents a wrinkle of the graphene film which can be formed by different thermal expansion coefficients of graphene and Cu metal. The narrow lines running from the upper left to lower right probably originated in surface morphology of the Cu film. The dark spots correspond to either metal nanoparticles or surface adsorbates that remain on the graphene surface.

The DF LEEM was measured for the same area, as shown in Figure 2e. The image was taken under the diffraction condition shown in the inset. The contrast of the DF image is quite uniform in the entire view, representing the single orientation of graphene in the measured area. Further measurement revealed that the diffraction pattern is unchanged after scanning ~1 mm. In addition, large area (0.2 mm) DF LEEM images also support the uniform growth of orientation-controlled graphene without a clear boundary (Supporting Information, SI-2). In the previous STM studies, it is proposed that there are two preferential graphene orientations on single-crystalline Cu(111) film; the angle between the [10] direction of graphene and the [101] direction of Cu(111) is 0° and 7°.^{38,42} Gao et al.

suggested that graphene domains with 0° orientation occupy 30% in the measured area.³⁸ Whereas, in our case, the rotation-free (i.e., 0° orientation) graphene extends to a very large area, occupying nearly 100%. Our optimized growth condition is supported to contribute the highly oriented single-layer graphene on heteroepitaxial Cu(111).

We further studied the transferred graphene by atomic force microscope (AFM) and Raman mapping measurements. From the AFM image shown in Figure 3a, the graphene was found to

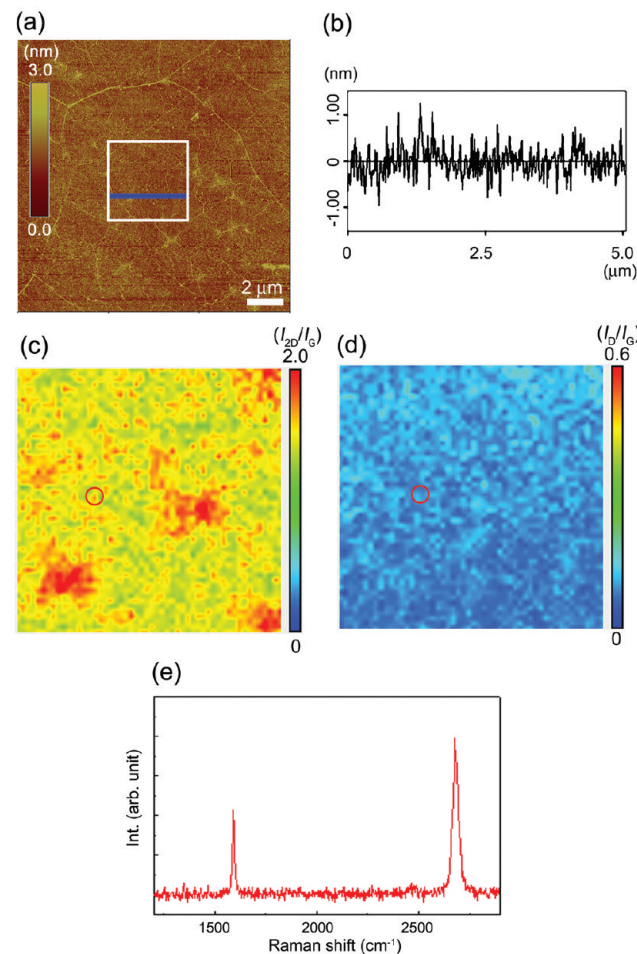


Figure 3. (a) AFM image of a graphene film transferred from Cu(111) onto the SiO₂/Si substrate. (b) Height profile measured by AFM along the blue line indicated in (a). Raman mapping images of the relative I_{2D}/I_G ratio (c) and I_D/I_G ratio (d). The measured $5 \times 5 \mu\text{m}$ area is indicated by the white square shown in (a). (e) Raman spectrum measured at the point marked in (c,d).

have a very smooth surface except for the linear wrinkles. The Raman mapping images of I_{2D}/I_G and I_D/I_G ratios are displayed in Figure 3c and 3d, respectively. Here, we used a 523 nm excitation laser line with spot size of around 600 nm. Although there are some fluctuations in the I_{2D}/I_G ratio, all the measured area gave a ratio higher than 1.5, supporting uniform single-layer graphene. As seen in the Raman spectra (Figure 3e), the D-band was negligible. The I_D/I_G mapping also supports that the D-band is weak in the whole $5 \mu\text{m} \times 5 \mu\text{m}$ measured area except for wrinkles (see Supporting Information, SI-3). Since the Raman D-band is associated with defects and domain boundary of a graphene film,³⁰ our epitaxial graphene film

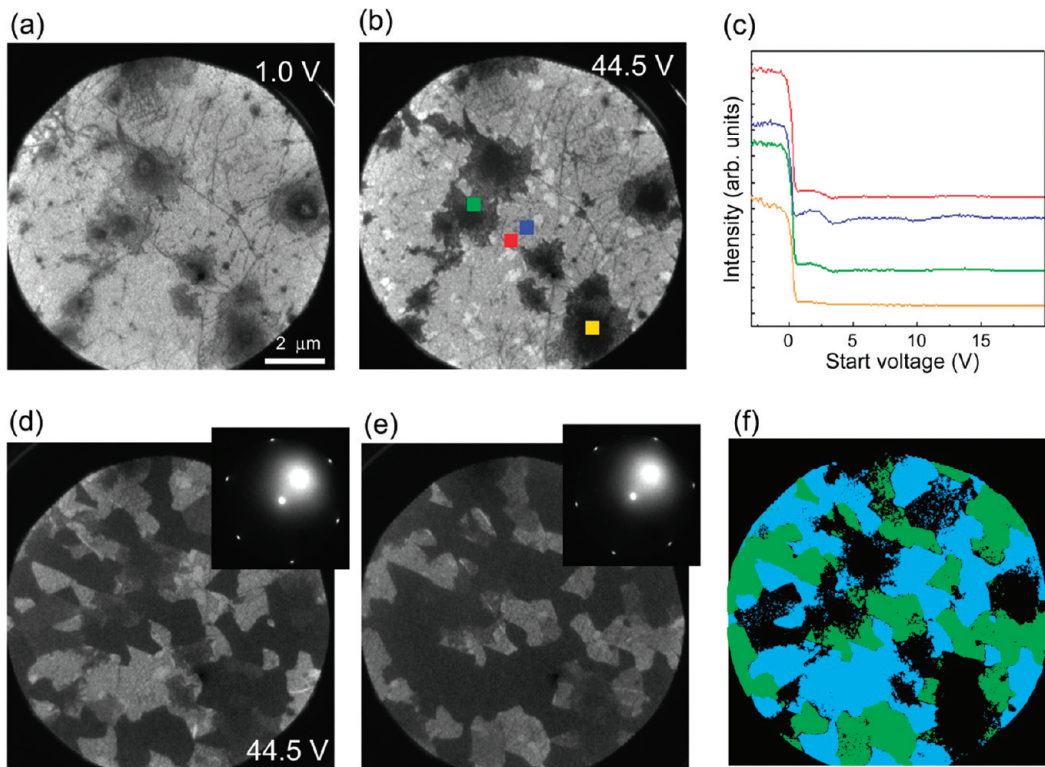


Figure 4. (a,b) BF LEEM images of graphene films grown on Cu(100) with 1.0 and 44.5 eV electron energies. (c) Electron reflectivity data measured at four different points marked in (b). (d,e) DF LEEM images of graphene measured under different diffraction conditions shown in the insets. (f) Spatial distribution of graphene domains determined from the DF LEEM images. The blue and green areas show the graphene domains rotated by 0° and 30° with respect to the underlying Cu lattice, respectively.

grown on Cu(111) might be free from the domain boundary based on the absence of D-band and the DF LEEM images.

We also performed LEEM measurement for the as-grown single-layer graphene on Cu(100), which can be regarded as a model system of widely studied Cu foil. Figure 4a,b shows BF LEEM images of the graphene on Cu(100) measured with different electron energies. The images show some dark contrasts with 1–2 μm size, and they became strong with the increase of energy. However, the electron reflectivity profiles (Figure 4c) indicate that the four points marked in Figure 4b are essentially the same, supporting the single-layer graphene for all the positions. This is consistent with the optical contrast shown in the Figure 1g inset that proves uniform single-layer graphene formation on the Cu(100) surface. There are two possible reasons for the observed dark contrast in the BF LEEM images. One reason is slight surface oxidation of the Cu surface; the surface oxidation slightly increases the work function of Cu metal that can give dark contrast in the BF image. This is plausible since we exposed our sample to air during transferring into the LEEM chamber. Another possibility is adsorption of impurities on the graphene surface; although we applied heat treatment prior to the LEEM measurement, the surface adsorbents are difficult to be removed completely from the graphene surface.

Interestingly, the DF LEEM images of graphene/Cu(100) (Figure 4d,e) showed a marked contrast to that of graphene on Cu(111) (see Figure 2e). We discovered that the as-grown graphene possesses a clear multidomain structure with patches of small domains. Under one selected diffraction condition, the mosaic structure appeared (Figure 4d), while the diffraction condition rotated by 30° gave a different mosaic pattern

(Figure 4e). This can be assigned to multiple graphene domain structures, similar to that reported by the dark field TEM analysis.^{18,19} The size of our graphene domains is below several micrometers, and domains form irregular boundaries. The domain structure was analyzed in terms of the domain orientation, as depicted in Figure 4f. The image analysis indicates that the graphene domains with 0° and 30° rotational angles occupy 46% and 34%, respectively. Note that these two orientations, 0° and 30° rotation, are crystallographically equivalent. When the misorientation of $\pm 2^\circ$ is allowed, the domains occupy 55% (for $0 \pm 2^\circ$) and 41% (for $30 \pm 2^\circ$), as shown in the Supporting Information, SI-4. We should note that most of the graphene domains prepared in our work have only two rotational directions, which are different from the previous graphene grown on Cu foil, in which a wide variation of rotational angles are observed.¹⁸ Being consistent with our epitaxial growth of graphene on the heteroepitaxial Cu(111), epitaxial graphene growth also occurs on the heteroepitaxial Cu(100) surface. Previous STM studies suggested graphene growth with specific orientations, 0°, 30°, and 6°, against the Cu(100) lattice,^{39–43} but here we demonstrate the distribution of the two major graphene domains quantitatively.

The wrinkle structure was also observed for the transferred graphene from Cu(100) by AFM and Raman D-band (Figure 5a; Supporting Information, SI-3). Except for this wrinkle structure, the growth of uniform single-layer graphene was confirmed by an optical microscope (see Figure 1g inset) and Raman mapping of the I_{2D}/I_G ratio (Figure 5c). However, the I_D/I_G mapping shown in Figure 5d indicates curved line features in the D-band intensity. As seen in Figure 5e, the D-band weakly appeared along the line. We note that no wrinkle

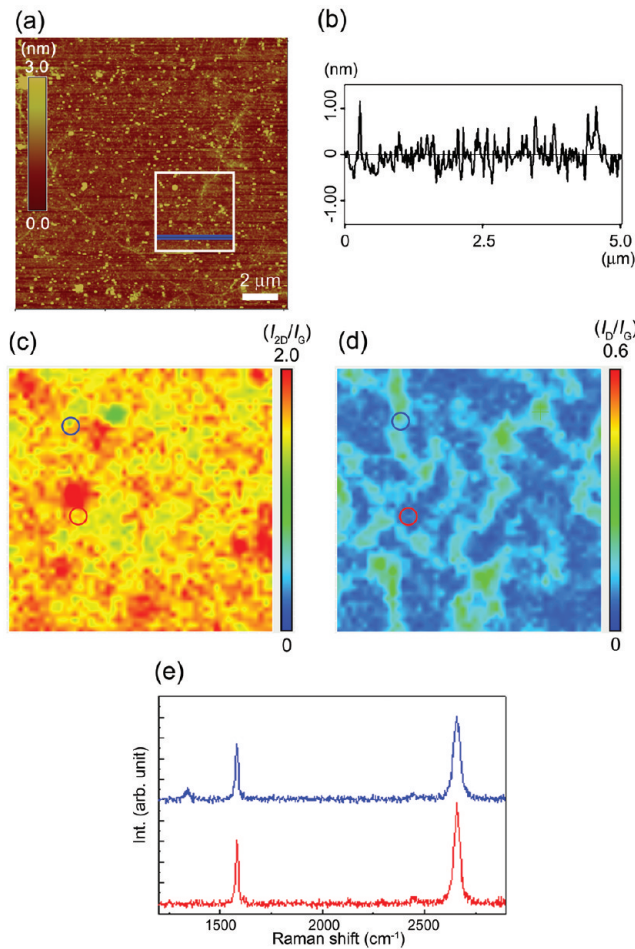


Figure 5. (a) AFM image of a graphene film transferred from Cu(100) onto the SiO₂/Si substrate. (b) Height profile measured along the blue line indicated in (a). Raman mapping images of I_{2D}/I_G (c) and I_D/I_G (d) ratios. The measured $5 \times 5 \mu\text{m}$ area is indicated by a white square shown in (a). (e) Raman spectra measured at the points marked in (c,d).

structure was observed by AFM for the mapped area. From the characteristic structure of the curved D-band image and the scale that are comparable to the DF LEEM images (see Figure 4d–f), we infer that the observed D-band reflects the domain boundary of graphene. When two adjacent graphene domains with 30° rotation meet at the boundary, the boundary cannot be atomically connected since the orientations of hexagons are different.

Finally, we discuss atomic models of graphene grown on Cu(111) and Cu(100) metals. Figure 6a represents the graphene epitaxially grown on Cu(111), as revealed by LEED and LEEM. The relative orientation is described as $[10]_{\text{graphene}}//[101]_{\text{Cu}(111)}$. A periodic moiré pattern is seen in Figure 6a, which is consistent with the previous STM image.³⁸ On the other hand, on Cu(100), there are two major orientations, $[10]_{\text{graphene}}//[011]_{\text{Cu}(100)}$ and $[01]_{\text{graphene}}//[011]_{\text{Cu}(100)}$. In both cases, C–C bonds of graphene hexagons are aligned parallel to the Cu–Cu bond of the topmost Cu surface. A stripe-like moiré pattern should appear as illustrated in Figure 6b because Cu(100) has 4-fold symmetry while graphene has 6-fold symmetry. This is experimentally verified by STM for the graphene on Cu foil.⁴¹ When graphene is grown on the Cu(100) surface, the grain boundary should

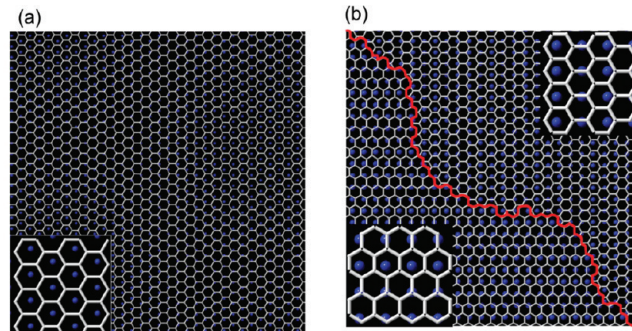


Figure 6. Atomic models of graphene grown on Cu(111) (a) and Cu(100) (b) surfaces. The graphene grown on Cu(111) is experimentally verified to have single orientation, while that on Cu(100) is found to have two orientations rotated by 30° . The red line in (b) represents a schematic of the domain boundary that is formed between two adjacent rotational domains.

remain due to the mis-oriented interface as illustrated in Figure 6b. The DF LEEM images (Figure 4d–f) clearly indicate the presence of domain boundaries. We think that this is the reason why the D-band was observed at the boundary (see Figure 5d) when the orientations of two adjacent graphene domains are not identical. In the case of single-layer graphene grown on Cu(111), all the graphene domain nuclei have the same hexagon orientation. Our LEEM and Raman results suggest that the boundary of the neighboring graphene domains grown on Cu(111) may be seamlessly connected during growth, in contrast to the graphene grown on Cu(100).

Recently, the domain boundary was studied by Raman mapping and scanning electron microscope (SEM) for the initial growth stage on Cu foil.³⁰ It was demonstrated that the graphene's domain boundary gives an observable D-band, when the hexagonal graphene nuclei meets at the boundary. Therefore, the absence of the D-band in the graphene on Cu(111) may indicate the boundary-free graphene growth. On the basis of STM observation, Lahiri et al. proposed the formation of one-dimensional defect lines for the graphene grown on Ni(111).⁴⁶ They suggested that a carbon octagon–pentagon pair is formed at the boundary even for the orientation-controlled graphene film. However, their growth temperature is much lower than the typical CVD temperature ($\sim 1000^\circ\text{C}$), and they used Ni metal as a catalyst; they synthesized graphene by annealing the ethylene-adsorbed Ni(111) substrate at 620°C for 30 min. We reported that the graphene grown on Cu at 900°C gives higher D-band intensity than that at 1000°C , implying significant defect or boundary formation at low growth temperature.³³ Moreover, the domain structure can depend on metal employed for the graphene growth.¹⁵ Therefore, the one-dimensional defect model proposed in the previous literature⁴⁶ cannot be simply applied to our system. However, since the lateral resolution of LEEM is not sufficient for the direct observation of atomic defects and/or domain boundaries, further microscopic study, such as TEM and STM, is necessary for atomic-scale understanding of the domain boundary in relation with the orientation of graphene hexagons.

In conclusion, we succeed in observing the domain structure and boundary in the CVD-grown graphene on heteroepitaxial Cu(111) and Cu(100) films by combining LEEM and Raman measurements. The heteroepitaxial Cu films give large-area, single-layer graphene film by ambient pressure CVD. The

graphene grown on Cu(111) is found to have single orientation in the large area with no detectable D-band except for wrinkles. In contrast, the graphene on Cu(100) exhibits a clear multidomain structure with two preferential domain orientations, reflecting the mismatch of the lattice symmetry of graphene (6-fold symmetry) and the Cu lattice (4-fold). The graphene boundary is detected by the Raman mapping measurement. This is due to the 30°-rotated adjacent domains which cannot be atomically connected. Most of the research works try to increase the graphene domain size through the optimization of CVD condition for Cu foils. In our method of CVD growth using heteroepitaxial single-crystalline Cu(111) film, the orientation of graphene nuclei is well controlled so that the boundary of domains might be atomically connected. Therefore, our work can present a new and alternative approach to grow "single-crystalline" graphene.

■ EXPERIMENTAL SECTION

Preparation of Heteroepitaxial Cu Films and Graphene Growth. Single-crystalline MgO(111) and (100) substrates were cleaned by sonicating in acetone and isopropyl alcohol. A 500 nm thick Cu film was deposited on these substrates with a power of 300 W in Ar atmosphere (0.6 Pa) by RF magnetron sputtering (Shibaura Mechatronics Corp., CFS-4ES). During sputtering, the substrate temperature was kept at 500 °C to promote epitaxial growth of the Cu film. For the ambient pressure CVD growth of graphene, the Cu film was annealed in mixed Ar 800 sccm and H₂ 14.2 sccm for 30 min at 1000 °C, followed by switching the gas to a mixture of CH₄ 0.5 sccm, H₂ 14.2 sccm, and Ar 800 sccm for 10 min. After CVD, the sample was rapidly cooled down to room temperature by taking out the sample from the furnace in the flow of Ar and H₂ gases.

Transfer to SiO₂/Si Substrate. As-grown graphene film was transferred to a target SiO₂(300 nm)/Si substrate by using PMMA, thermal tape, and etching solution.¹⁵ After CVD, the surface of graphene film was covered with PMMA by spin-coating. The thin PMMA was mechanically supported with thermal tape (Revalpha, Nitto-Denko). Then, Cu film was dissolved with aqueous solution containing FeCl₃ and HCl to release the graphene supported with PMMA and thermal tape. The thermal tape/PMMA/graphene stack was washed with deionized water and placed on the SiO₂/Si substrate. Finally, the thermal tape was removed by heating at 120 °C, followed by PMMA removal with acetone.

Characterizations. The crystallinity of heteroepitaxial Cu films was measured by XRD (Rigaku, RINT 2500) and SEM (Zeiss, Ultra55) equipped with EBSD (TSL Solutions, OIM). Crystal orientations of as-grown graphene films were characterized by LEED and LEEM equipment. LEED patterns of as-grown graphene were recorded in a UHV chamber of 8 × 10⁻⁹ Pa with a Spectaleed (Omicron, Germany) instrument. LEEM images and spectra were measured with Elmitec LEEM III. To remove impurities on the surface, we applied thermal annealing in a vacuum before the measurement. Transferred graphene films were analyzed by an optical microscope, AFM (Bruker, Nanoscope IIIa), and a Raman spectrometer (Tokyo Instruments, Nanofinder30).

■ ASSOCIATED CONTENT

S Supporting Information

Other LEED and LEEM data, Raman mapping and AFM images for the wrinkle structure, and orientation analysis data.

This material is available free of charge via the Internet at <http://pubs.acs.org>.

■ AUTHOR INFORMATION

Corresponding Author

*E-mail: ago@cm.kyushu-u.ac.jp.

■ ACKNOWLEDGMENTS

This work was supported by JSPS Funding Program for Next Generation World-Leading Researchers (NEXT Program). Y.O. acknowledges the support from the Global Center of Excellence (GCOE) of Novel Carbon Resource Sciences at Kyusyu University.

■ REFERENCES

- (1) Geim, A. K.; Novoselov, K. S. The Rise of Graphene. *Nat. Mater.* **2007**, *6*, 183–191.
- (2) Bae, S.; Kim, H.; Lee, Y.; Xu, X.; Park, J. S.; Zheng, Y.; Balakrishnan, J.; Lei, T.; Kim, H. R.; Song, Y. I.; et al. Roll-to-Roll Production of 30-in. Graphene Films for Transparent Electrodes. *Nat. Nanotechnol.* **2010**, *5*, 574–578.
- (3) De Arco, L. G.; Zhang, Y.; Schlenker, C. W.; Ryu, K.; Thompson, M. E.; Zhou, C. Continuous, Highly Flexible, and Transparent Graphene Films by Chemical Vapor Deposition for Organic Photovoltaics. *ACS Nano* **2010**, *4*, 2865–2873.
- (4) Lin, Y. M.; Dimitrakopoulos, C.; Jenkins, K. A.; Farmer, D. B.; Chiu, H. Y.; Grill, A.; Avouris, P. 100-GHz Transistors from Wafer-Scale Epitaxial Graphene. *Science* **2010**, *327*, 662.
- (5) Geim, A. K. Graphene: Status and Prospects. *Science* **2009**, *324*, 1530–1534.
- (6) Novoselov, K. S.; Geim, A. K.; Morozov, S. V.; Jiang, D.; Zhang, Y.; Dubonos, S. V.; Grigorieva, I. V.; Firsov, A. A. Electric Field Effect in Atomically Thin Carbon Films. *Science* **2004**, *306*, 666–669.
- (7) Berger, C.; Song, Z.; Li, X.; Wu, X.; Brown, N.; Naud, C.; Mayou, D.; Li, T.; Hass, J.; Marchenkov, A. N.; et al. Electronic Confinement and Coherence in Patterned Epitaxial Graphene. *Science* **2006**, *312*, 1191–1196.
- (8) Emtsev, K. V.; Bostwick, A.; Horn, K.; Jobst, J.; Kellogg, G. L.; Ley, L.; McChesney, J. L.; Ohta, T.; Reshanov, S. A.; Röhrl, J.; et al. Towards Wafer-Size Graphene Layers by Atmospheric Pressure Graphitization of Silicon Carbide. *Nat. Mater.* **2009**, *8*, 203–207.
- (9) Hibino, H.; Kageshima, H.; Maeda, F.; Nagase, M.; Kobayashi, Y.; Yamaguchi, H. Microscopic Thickness Determination of Thin Graphite Films formed on SiC from Quantized Oscillation in Reflectivity of Low-Energy Electrons. *Phys. Rev. B* **2008**, *77*, 75413.
- (10) Gilje, S.; Han, S.; Wang, M.; Wang, K. L.; Kaner, R. B. A. Chemical Route to Graphene for Device Applications. *Nano Lett.* **2007**, *7*, 3394–3398.
- (11) Eda, G.; Fanchini, G.; Chhowalla, M. Large-Area Ultrathin Films of Reduced Graphene Oxide as a Transparent and Flexible Electronic Material. *Nat. Nanotechnol.* **2008**, *3*, 270–274.
- (12) Yu, Q.; Lian, J.; Siriponglert, S.; Li, H.; Chen, Y. P.; Pei, S. S. Graphene Segregated on Ni Surfaces and Transferred to Insulators. *Appl. Phys. Lett.* **2008**, *93*, 113103.
- (13) Reina, A.; Jia, X.; Ho, J.; Nezich, D.; Son, H.; Bulovic, V.; Dresselhaus, M. S.; Kong, J. Large Area, Few-Layer Graphene Films on Arbitrary Substrates by Chemical Vapor Deposition. *Nano Lett.* **2009**, *9*, 30–35.
- (14) Kim, K. S.; Zhao, Y.; Jang, H.; Lee, S. Y.; Kim, J. M.; Kim, K. S.; Ahn, J. H.; Kim, P.; Choi, J. Y.; Hong, B. H. Large-Scale Pattern Growth of Graphene Films for Stretchable Transparent Electrodes. *Nature* **2009**, *457*, 706–710.
- (15) Ago, H.; Ito, Y.; Mizuta, N.; Yoshida, K.; Hu, B.; Orofeo, C. M.; Tsuji, M.; Ikeda, K.; Mizuno, S. Epitaxial Chemical Vapor Deposition Growth of Single-Layer Graphene over Cobalt Film Crystallized on Sapphire. *ACS Nano* **2010**, *4*, 7407–7414.

- (16) Coraux, J.; N'Diaye, A. T.; Busse, C.; Michely, T. Structural Coherency of Graphene on Ir(111). *Nano Lett.* **2008**, *8*, 565–570.
- (17) Li, X.; Cai, W.; An, J.; Kim, S.; Nah, J.; Yang, D.; Piner, R.; Velamakanni, A.; Jung, I.; Tutuc, E.; et al. Large-Area Synthesis of High-Quality and Uniform Graphene Films on Copper Foils. *Science* **2009**, *324*, 1312–1314.
- (18) Huang, P. Y.; Ruiz-Vargas, C. S.; van der Zande, A. M.; Whitney, W. S.; Levendorf, M. P.; Kevek, J. W.; Garg, S.; Alden, J. S.; Hustedt, C. J.; Zhu, Y. Grains and Grain Boundaries in Single-Layer Graphene Atomic Patchwork Quilts. *Nature* **2011**, *469*, 389–393.
- (19) Kim, K.; Lee, Z.; Regan, W.; Kisielowski, C.; Crommie, M. F.; Zettl, A. Grain Boundary Mapping in Polycrystalline Graphene. *ACS Nano* **2011**, *5*, 2142–2146.
- (20) An, J.; Voelkl, E.; Suk, J. W.; Li, X.; Magnuson, C. W.; Fu, L.; Tiemeijer, P.; Bischoff, M.; Freitag, B.; Popova, E.; et al. Domain (Grain) Boundaries and Evidence of “Twin Like” Structures in Chemical Vapor Deposited Grown Graphene. *ACS Nano* **2011**, *5*, 2433–2439.
- (21) Wofford, J. M.; Nie, S.; McCarty, K. F.; Bartelt, N. C.; Dubon, O. D. Graphene Islands on Cu Foils: The Interplay between Shape, Orientation, and Defects. *Nano Lett.* **2010**, *10*, 4890–4896.
- (22) Li, X.; Magnuson, C. W.; Venugopal, A.; An, J.; Suk, J. W.; Han, B.; Borysiak, M.; Cai, W.; Velamakanni, A.; Zhu, Y.; et al. Graphene Films with Large Domain Size by a Two-Step Chemical Vapor Deposition Process. *Nano Lett.* **2010**, *10*, 4328–4334.
- (23) Robertson, A. W.; Warner, J. H. Hexagonal Single Crystal Domains of Few-Layer Graphene on Copper Foils. *Nano Lett.* **2011**, *11*, 1182–1189.
- (24) Yazyev, O. V.; Louie, S. G. Electronic Transport in Polycrystalline Graphene. *Nat. Mater.* **2010**, *9*, 806–809.
- (25) Malola, S.; Häkkinen, H.; Koskinen, P. Structural, Chemical, and Dynamical Trends in Graphene Grain Boundaries. *Phys. Rev. B* **2010**, *81*, 165447.
- (26) Grantab, R.; Shenoy, V. B.; Ruoff, R. S. Anomalous Strength Characteristics of Tilt Grain Boundaries in Graphene. *Science* **2010**, *330*, 946–948.
- (27) Yazyev, O. V.; Louie, S. G. Topological Defects in Graphene: Dislocations and Grain Boundaries. *Phys. Rev. B* **2010**, *81*, 195420.
- (28) Červenka, J.; Katsnelson, M. I.; Flipse, C. F. J. Room-Temperature Ferromagnetism in Graphite Driven by Two-Dimensional Networks of Point Defects. *Nat. Phys.* **2009**, *5*, 840–844.
- (29) Li, X.; Magnuson, C. W.; Venugopal, A.; Tromp, R. M.; Hannon, J. B.; Vogel, E. M.; Colombo, L.; Ruoff, R. S. Large-Area Graphene Single Crystals Grown by Low-Pressure Chemical Vapor Deposition of Methane on Copper. *J. Am. Chem. Soc.* **2011**, *133*, 2816–2819.
- (30) Yu, Q.; Jauregui, L. A.; Wu, W.; Colby, R.; Tian, J.; Su, Z.; Cao, H.; Liu, Z.; Pandey, D.; Wei, D.; et al. Control and Characterization of Individual Grains and Grain Boundaries in Graphene Grown by Chemical Vapour Deposition. *Nat. Mater.* **2011**, *10*, 443–449.
- (31) Vlassiouk, I.; Regmi, M.; Fulvio, P.; Dai, S.; Datskos, P.; Eres, G.; Smirnov, S. Role of Hydrogen in Chemical Vapor Deposition Growth of Large Single-Crystal Graphene. *ACS Nano* **2011**, *5*, 6069–6076.
- (32) Iwasaki, T.; Park, H. J.; Konuma, M.; Lee, D. S.; Smet, J. H.; Starke, U. Long-Range Ordered Single-Crystal Graphene on High-Quality Heteroepitaxial Ni Thin Films Grown on MgO(111). *Nano Lett.* **2011**, *11*, 79–84.
- (33) Hu, B.; Ago, H.; Ito, Y.; Kawahara, K.; Tsuji, M.; Magome, E.; Sumitani, K.; Mizuta, N.; Ikeda, K.; Mizuno, S. Epitaxial Growth of Large-Area Single-Layer Graphene over Cu(111)/sapphire by Atmospheric Pressure CVD. *Carbon* **2012**, *50*, 57–65.
- (34) Reddy, K. M.; Gledhill, A. D.; Chen, C. H.; Drexler, J. M.; Padturea, N. P. High Quality, Transferrable Graphene Grown on Single Crystal Cu(111) Thin Films on Basal-Plane Sapphire. *Appl. Phys. Lett.* **2011**, *98*, 113117.
- (35) Van, C. V.; Kimouche, A.; Plantey, A. R.; Fruchart, O.; Guillemaud, P. B.; Bendiab, N.; Coraux, J. Epitaxial Graphene Prepared by Chemical Vapor Deposition on Single Crystal Thin Iridium Films on Sapphire. *Appl. Phys. Lett.* **2011**, *98*, 181903.
- (36) Sutter, P. W.; Albrecht, P. M.; Sutter, E. A. Graphene Growth on Epitaxial Ru Thin Films on Sapphire. *Appl. Phys. Lett.* **2010**, *97*, 213101.
- (37) Yoshii, S.; Nozawa, K.; Toyoda, K.; Matsukawa, N.; Odagawa, A.; Tsujimura, A. Suppression of Inhomogeneous Segregation in Graphene Growth on Epitaxial Metal Films. *Nano Lett.* **2011**, *11*, 2628–2633.
- (38) Gao, L.; Guest, J. R.; Guisinger, N. P. Epitaxial Graphene on Cu (111). *Nano Lett.* **2010**, *10*, 3512–3516.
- (39) Rasool, H. I.; Song, E. B.; Allen, M. J.; Wassei, J. K.; Kaner, R. B.; Wang, K. L.; Weiller, B. H.; Gimzewski, J. K. Continuity of Graphene on Polycrystalline Copper. *Nano Lett.* **2011**, *11*, 251–256.
- (40) Zhang, Y.; Gao, T.; Gao, Y.; Xie, S.; Ji, Q.; Yan, K.; Peng, H.; Liu, Z. Defect-Like Structures of Graphene on Copper Foils for Strain Relief Investigated by High-Resolution Scanning Tunneling Microscopy. *ACS Nano* **2011**, *5*, 4014–4022.
- (41) Cho, J.; Gao, L.; Tian, J.; Cao, H.; Wu, W.; Yu, Q.; Yitamben, E. N.; Fisher, B.; Guest, J. R.; Chen, Y. P.; et al. Atomic-Scale Investigation of Graphene Grown on Cu Foil and the Effects of Thermal Annealing. *ACS Nano* **2011**, *5*, 3607–3613.
- (42) Zhao, L.; Rim, K. T.; Zhou, H.; He, R.; Heinz, T. F.; Pinczuk, A.; Flynn, G. W.; Pasupathy, A. N. Influence of Copper Crystal Surface on the CVD Growth of Large Area Monolayer Graphene. *Solid State Commun.* **2011**, *151*, 509–513.
- (43) Rasool, H. I.; Song, E. B.; Mecklenburg, M.; Regan, B. C.; Wang, K. L.; Weiller, B. H.; Gimzewski, J. K. Atomic-Scale Characterization of Graphene Grown on Copper (100) Single Crystals. *J. Am. Chem. Soc.* **2011**, *133*, 12536–12543.
- (44) Reina, A.; Thiele, S.; Jia, X.; Bhaviripudi, S.; Dresselhaus, M. S.; Schaefer, J. A.; Kong, J. Growth of Large-Area Single- and Bi-Layer Graphene by Controlled Carbon Precipitation on Polycrystalline Ni Surfaces. *Nano Res.* **2009**, *2*, 509–516.
- (45) Orofeo, C. M.; Ago, H.; Hu, B.; Tsuji, M. Synthesis of Large-Area, Homogeneous, Single Layer Graphene by Annealing Amorphous Carbon on Co and Ni. *Nano Res.* **2011**, *4*, 531–540.
- (46) Lahiri, J.; Lin, Y.; Bozkurt, P.; Oleynik, I. I.; Batzill, M. An Extended Defect in Graphene As a Metallic Wire. *Nat. Nanotechnol.* **2010**, *5*, 326–329.